applied sciences

MDPI

Article

Research on Cutting Temperature of GH4169 Turning with Micro-Textured Tools

Xinmin Feng, Xiwen Fan, Jingshu Hu * and Jiaxuan Wei

Key Laboratory of Advanced Manufacturing Intelligent Technology, Ministry of Education, Harbin University of Science and Technology, Harbin 150080, China; sxfxmin@163.com (X.F.); 17780924565@139.com (X.F.)
* Correspondence: hjs4600@163.com; Tel.: +86-15846009563

Abstract: The GH4169 superalloy has the characteristics of high strength, strong thermal stability, large specific heat capacity, small thermal conductivity, etc., but it is also a typical hard-to-cut material. When cutting this material with ordinary cutting tools, the cutting force is large, and the cutting temperature is high, which leads to severe tool wear and short service life. In order to improve the performance of tools when cutting GH4169, reduce the cutting temperature, and extend the service life of the tool, micro-textured tools were used to cut GH4169 in spray cooling. The effects of micro-texture morphology and dimensional parameters on cutting temperature were analyzed. Firstly, tools with micro-textures of five different morphologies were designed near the nose on the rake face of the cemented carbide tools. The three-dimensional cutting models of the micro-textured tools with different morphologies were established by using ABAQUS, and a simulation analysis was carried out. Compared with the non-textured tools, the micro-texture morphology with the lowest cutting temperature was selected according to the simulation results of the cutting temperature. Secondly, based on the optimized morphology, tools with micro-textures of different size parameters were designed. When cutting GH4169, the cutting temperature of the tools was simulated and analyzed, and the size parameters of the micro-textured tools with the lowest cutting temperature were selected as well. Finally, the designed micro-textured tools were processed and applied in cutting experiments. The simulation model was verified in the experiments, and the influence of size parameters of micro-textures on the cutting temperature was analyzed. This paper provides a theoretical reference and basis for cutting GH4169 and the design and application of micro-textured tools.

Keywords: micro-texture; cutting parameters; temperature; finite element simulation; GH4169

Citation: Feng, X.; Fan, X.; Hu, J.; Wei, J. Research on Cutting Temperature of GH4169 Turning with Micro-Textured Tools. *Appl. Sci.* **2023**, *13*, 6832. https://doi.org/10.3390/app13116832

Academic Editor: Wei Li

Received: 20 April 2023
Revised: 27 May 2023
Accepted: 2 June 2023
Published: 5 June 2023

1. Introduction

The nickel-based superalloy GH4169 has strong thermal strength, thermal stability, and thermal fatigue properties. It is widely used in the aerospace field [1,2]. However, GH4169 is a typical difficult-to-machine material. In the process of cutting GH4169, the commonly used tools are often accompanied by harsh working conditions. In the cutting process, the cutting temperature of the tool is very high, so it will change the friction coefficient of the rake face and the performance of the workpiece material, and affect the size of the built-up edge. All of these aspects will directly influence the service life of the tool. In addition, it can also cause problems such as an unsatisfactory surface quality of the processed workpiece and a failure to achieve the expected accuracy [3].

To solve the problem of high tool temperature in cutting, many scholars have used different cooling technologies to cool down the cutting environment, such as low-temperature cooling technology [4], high-pressure cooling technology [5,6], and spray cooling technology [7].

In addition, with the continuous development of science and technology, a micro-textured tool with excellent cutting performance has been favored by scholars in recent years, which can reduce the cutting temperature, cutting force, and friction coefficient, and improve the surface quality of the machined workpiece.

Micro-textured tools originate from bionic tribology [8]. They are tools with a rake face/flank that is designed and manufactured with micro-grooves, micro-pits, or other surface textures of reasonable shape and arrangement by means of micro-machining techniques such as the electric spark, lithography, and laser techniques. In the process of cutting, the insertion of the structure reduces the contact length between the tool and the chips and increases the heat dissipation area of the tool surface, thereby reducing the friction coefficient, cutting temperature, and cutting force. Moreover, it also improves the machined surface quality of the workpiece, prolongs tool life, and reduces energy consumption [9–11].

In recent years, many scholars have conducted a lot of research on micro-textured tools with different morphologies and size parameters to improve cutting performance and reduce cutting temperature:

Some scholars have studied the effect of micro-textures on the cutting performance of tools. For instance, Rao et al. investigated the influence of micro-textured tools on the cutting performance of Ti-6Al-4V titanium alloy with finite element simulation and experiments. Through the research, it was found that in the same cutting conditions, the cutting temperature of the micro-textured tools decreased by 30% [12]. Zhang et al. studied the cutting performance of the micro-textured tools when cutting Ti-6Al-4V. Through theoretical analysis and experiments, it was verified that the micro-textured tools can effectively improve the lubrication performance and reduce the cutting temperature in machining [13]. Liu et al. studied the cutting performance of the micro-textured WC-10Ni3Al tools when cutting Ti-6Al-4V. It was found that, compared with the non-textured tools, micro-textured WC-10Ni3Al tools can store lubricating oil and promote lubricating oil penetration in the process of cutting, thus significantly reducing the cutting temperature in the process of processing [14]. WU et al. conducted a comparative study on the cutting performance of non-textured and micro-textured tools in cutting Ti-6AL-4V using ABAQUS finite element simulation and experiments. They found that the cutting temperature of micro-textured tools decreased by 5–25% during cutting [15].

Moreover, scholars also studied the influence of micro-textured tools with different morphologies on cutting performance. Sun et al. studied the influence of micro-pit and micro-groove composite textures on the cutting performance of WC/Co-based cemented tools when cutting pure iron, and the experimental results found that the cutting temperatures of micro-textured tools were significantly lower than that of non-textured tools, and compared with a single micro-texture, the cutting temperatures of composite micro-textures were reduced by 7.1~33.3% [16]. Feng et al. designed ceramic micro-textured tools with different morphologies (MST-0, MST-1, MST-2), and conducted finite element simulation on the cutting of Al2O3-TiC composite materials using micro-textured tools with AdvantEdge. After comparison and verification with experiments, it was found that the cutting temperature of MST-2 micro-textured tools was the lowest compared with traditional non-textured tools (MST-0) [17]. AlaaOleak et al. designed micro-textured tools with different morphologies, and based on three-dimensional finite element simulation, studied the impact of micro-textures with different morphologies on the cutting performance of tools when cutting titanium alloys. Otherwise, it was found that pit micro-textured tools have the best cooling effect, and compared with non-textured tools, the high-temperature area of micro-textured tools is significantly less than that of non-textured tools [18].

In addition, some scholars have studied the influence of micro-textured tools with different size parameters on cutting performance. For example, Yang et al. studied the cutting temperature of micro-textured ball end milling cutters with different size parameters when milling the titanium alloy by combining finite element simulation and experimental verification. The optimal parameters of the micro-circular pit texture were obtained as follows: the diameter of the micro-circular pit was 40 microns, pit spacing was 225 microns, the distance from the cutting edge was 100 microns, and the radius of the blunt edge was 60 microns [19]. Li et al. analyzed the influence of width, spacing, edge distance, and depth of micro-texture on the main cutting force and cutting temperature of the tool when cutting Ti-6AL-4V. The results showed that when the width of the micro-texture was 40 μm, the edge distance was 80 μm, the spacing was 70 μm, the depth was 20 μm, and the cutting temperature of the tool was the lowest [20].

There are also some scholars that have conducted relevant research on the distribution mode of micro-textures. D et al. simulated the cutting process of cutting Ti-6Al-4V with micro-textured WC/Co tools by using DEFORM 3D finite element simulation with SAE 40 as a semi-solid lubricant, and studied the influence law of cutting Ti-6Al-4V with micro-textured tools. Finally, combined with the turning experiment, it was found that the cutting temperature of micro-textured tools decreased to different degrees during the cutting process. This effect was more apparent when cutting with micro-textured tools of the vertical shape [21]. Wang et al. simulated the cutting of medium carbon steel AISI 1045 with micro-textured tools. It was found that the cooling effect of the lateral micro-textured tool was more apparent compared with non-textured tools, and it showed good chip fragility in the process of cutting [22].

To conclude, reasonable shapes, structures, and arrangements of micro-textures on the surface of the tool can reduce the cutting temperature in the actual cutting process. However, for research on the cutting performance of micro-textured tools, the cooling effect of micro-textured tools with different morphologies and size parameters is also different when cutting different materials. At present, most research on cutting materials is focused on titanium alloy, with only a small number of pure iron and medium carbon steel. There is little research on the cutting of GH4169 using micro-structured tools in spray cooling conditions, and there is even less research on the influence of the morphology, size parameters, and arrangement of micro-structured tools on the cutting temperature when cutting GH4169.

Based on the above problems, the cutting temperature of GH4169 with micro-textured tools of different morphologies and size parameters was studied by a combination of simulations and experiments in spray cooling. Firstly, five types of micro-textures with different morphologies were designed on the rake face of the tools. The simulation models of the micro-textured tools cutting GH4169 were established and simulated in ABAQUS, and the morphology of the micro-texture with the lowest cutting temperature was selected. Secondly, based on the optimal micro-texture morphology, an orthogonal simulation scheme for micro-texture size parameters was designed, and a cutting simulation was conducted to analyze and select the combination of micro-texture size parameters with the lowest cutting temperature. Finally, the micro-textured tools were processed using a femtosecond laser, and cutting experiments were conducted in spray cooling, which verified the previous simulation analysis results and ultimately obtained the influence of the micro-texture parameters on the cutting temperature. These studies will provide guidance for the efficient machining of GH4169 and the design and application of micro-textured tools.

2. Finite Element Modeling of Micro-Textured Tool for Cutting GH4169

2.1. The Establishment of Geometric Models

In the process of cutting, the cutting heat is mainly focused on the tool nose. In this study, only the part of the carbide tool that was in contact with the chips was established to simplify the geometric model of the tool. To ensure that the processing of micro-textures was not affected by grooves, a flat insert was selected. Then, a matching shank was selected. The insert was installed on the shank, with a rake angle of $-5°$ and a clearance angle of $5°$ in cutting, so the tool rake angle was set as $-5°$ and the tool clearance angle was set as $5°$ in this study. The parameters related to the YG8 tool are shown in Table 1.

Table 1. Material properties of cutting tools.

Tool Material	Density (g/cm^3)	Young's Modulus (Gpa)	Poisson's Ratio	Linear Expansivity (m/m°C)	Specific Heat (J/kg·°C)	Thermal Conductivity (W/m^2·K)
Carbide	14.6	640	0.22	4.5×10^{-7}	220	75.4

Due to the severe friction, high temperatures were generated on the rake face and flank face of the tools when cutting GH4169. In order to study the influence of the existence of micro-textures on the cutting temperature distribution of the tool and the temperature variation in the contact area between the tool and the chips, the micro-texture distribution was set in the range of 500 μm from the tool nose in this paper. The area occupancy of the micro-texture was 20%, and the depth was 20 μm. Based on the flow characteristics of the chips during cutting, five types of morphologies of micro-textures were designed, as shown in Figure 1. T1, a micro-pit textured tool, has micro-pits arranged in a circular arc shape on the rake surface near the tool nose, similar to the surface microstructure of a dung beetle shell; T2, a micro-pyramid textured tool, has micro-grooves on the rake face near the tool nose, similar to the rib-like texture of a shark's skin; T3, a micro-groove-parallel textured tool, has linear micro-grooves that are approximately parallel to the arc of the tool nose, similar to the surface groove structure of clam shells; T4, a micro-groove-vertical textured tool, has a micro-groove structure that is approximately perpendicular to the arc of the tool nose, similar to the surface groove structure of a clam shell rotated 90°; T5, a micro-elliptical textured tool, has circular grooves on the rake face near the tool nose, similar to the microstructure of pangolin scales.

The size parameters of the micro-texture shapes are shown in Table 2, namely: the distance from the micro-pits (micro-groove) to the tool nose arc (edge distance *A*), the distance between the micro-pits (micro-groove) (spacing *B*), and other dimensions (diameter, long/short axis, length/width) (parameter *C*). The micro-texture shapes designed in this section are shown in Figure 1.

Table 2. Micro-texture size parameters of different morphologies.

Tool Number	*A*/μm	*B*/μm	*C* (*c*1, *c*2, *C*1, *C*2)/μm
T1	120	90	40
T2	120	70	80, 40
T3	120	70	50, 450
T4	120	70	450, 50
T5	120	30	120, 240, 300, 600

2.2. Material Constitutive Model

In response to the high-thermoplastic, creep, thermal stability, and stress-strengthening characteristics of GH4169, this paper adopts the Johnson–Cook material constitutive model, whose mathematical expression is as follows [23]:

$$\sigma = [A + B\varepsilon^n]\left[1 + C\ln\frac{\dot{\varepsilon}}{\dot{\varepsilon}_0}\right]\left[1 - \left(\frac{T - T_r}{T_m - T_r}\right)^m\right] \quad (1)$$

where *A* is the yield strength (Mpa) of the material; *B* is the hardening modulus (Mpa) of the material; *C* is the strain rate strength coefficient; *M* is the thermal softening coefficient; *N* is the strain-strengthening coefficient; ε is equivalent plastic strain; $\overline{\varepsilon}$ is the equivalent plastic strain rate; $\overline{\varepsilon}_0$ is the quasi-static strain rate; T_r is the melting point temperature of the material; and T_0 is the ambient temperature. Meanwhile, the plastic parameters *A*, *B*, *n*, *c*, and *m* of the material can be obtained from the SHPB split Hopkinson bar experiment and quasi-static experiment of smooth specimens, and the equivalent strain rate can be obtained by fitting the average values of the compression bar, tension, and torsion experiments.

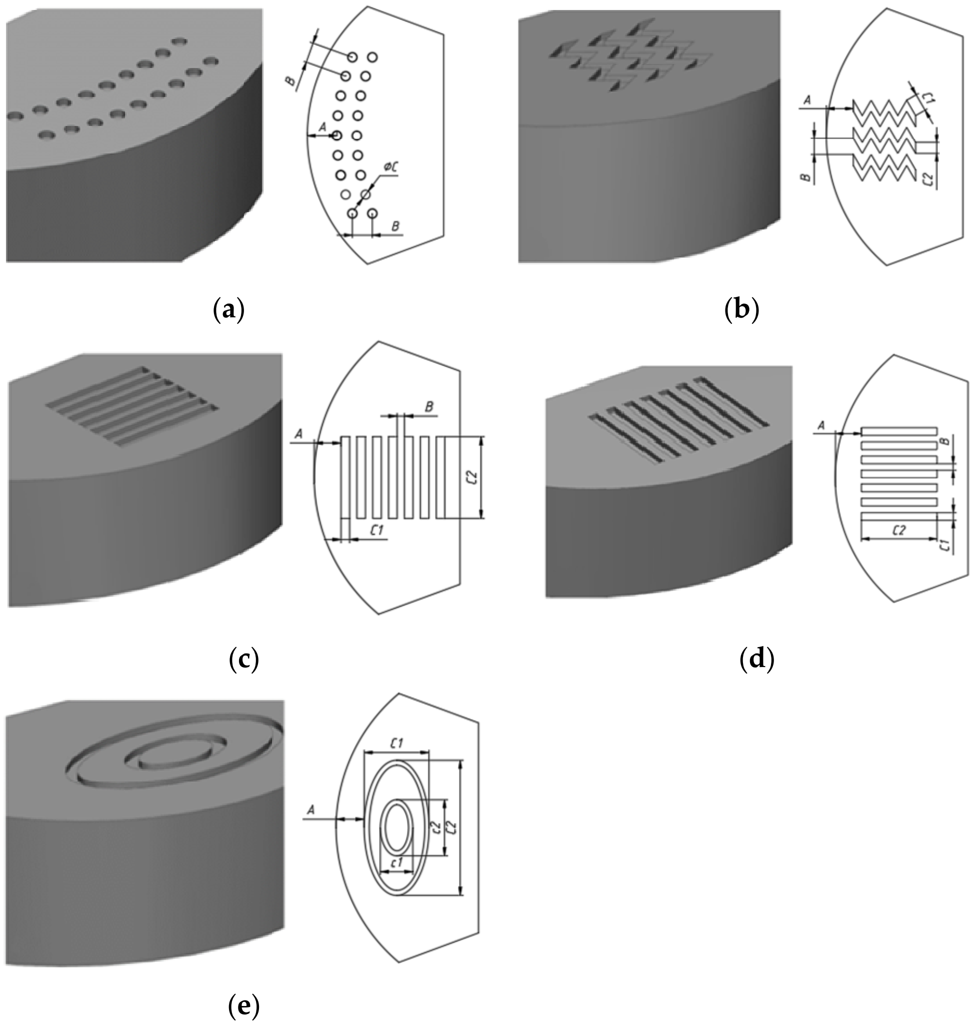

Figure 1. Schematic diagram of micro-texture shapes and parameters: (**a**) micro-pit; (**b**) micro-pyramids; (**c**) micro-groove-parallel; (**d**) micro-groove-vertical; (**e**) micro-elliptical.

Johnson–Cook constitutive model parameters of GH4169 are shown in Table 3.

Table 3. J–C constitutive model parameters of GH4169.

Materials	*A*/Mpa	*B*/Mpa	*m*	*c*	*n*	T_m/°C
GH4169	860	683	1	0.01	0.47	1260

Johnson–Cook shear failure criterion was adopted as the failure criterion. The values of parameters defined in the Johnson–Cook dynamic failure model are shown in Table 4 [24].

Table 4. J–C failure parameters of GH4169.

Failure Criterion	d_1	d_2	d_3	d_4	d_5
Value	0.11	0.75	−1.45	0.04	0.89

2.3. Mesh

The meshing method used in this paper was a combination of free mesh and sweeping mesh, and the linear reduced integral element was selected as the solid element(C3D8R) [25]. To ensure accuracy, reduce the number of dividing units, and meet the mesh density and unit type, the micro-texture structure was divided into N regions. The unit type was the temperature–displacement coupling. Hexahedral units (Hex), which can ensure the accuracy of the model, stability of the model, and computational efficiency and are easy to generate and process, were used for dividing, and the neutral axis algorithm, which is easier to obtain a regular shape mesh, was selected. The mesh is shown in Figure 2.

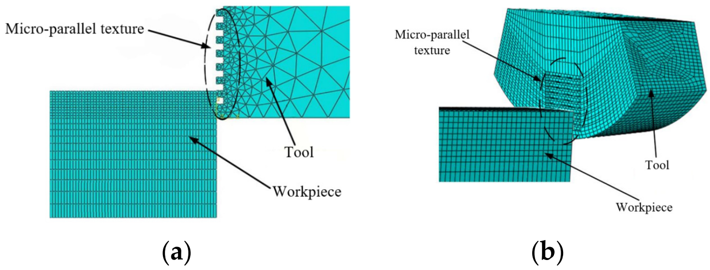

Figure 2. Meshing of the cutting model: (**a**) meshing (two-dimensional cutting model); (**b**) meshing (three-dimensional cutting model).

2.4. Setting Coefficient of Heat Transfer

The experiment was carried out in spray cooling. In order to consider the effect of spray cooling, the coefficient of heat transfer was introduced in the simulation model.Combining with ANSYS, DEFORM, and previous research, the range of heat transfer coefficient h was 2400–2700 (W/m^2·K) when cutting GH4169 in a constant spray pressure and the flow rate [26].

3. Simulation Analysis of Cutting Temperature for Micro-Textured Tools with Different Morphologies

According to the previous experiment for GH4169, in order to minimize the cutting force, the cutting parameters set in the cutting simulation model were as follows: the cutting speed v was 50 m/min, the feed rate f was 0.2 mm/r, the cutting depth a_p was 0.2 mm, and the environmental temperature was set as 25 °C. Under the set cutting parameters, the cutting simulation of GH4169 using micro-textured tools with different morphologies was carried out.

Figure 3 shows the distribution of temperature of the tool and workpiece in the turning process under the same working conditions. It was easily found that the high-temperature area is concentrated in the contact area of the tool–chip and diffuses step by step from the tool nose. It can be seen from the tool nose that the temperature of tool T3 is significantly lower than that of the non-textured tool, and it may have also formed C-shaped chips earlier. In other words, the micro-textured tool with a parallel groove to the tool nose can increase the unit curl degree of chips, and the effect of the chips breaking should be better.

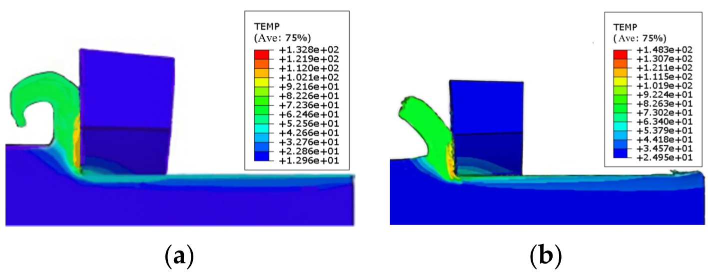

Figure 3. Temperature field of tool and workpiece: (**a**) micro-pit tool; (**b**) non-textured tool.

Figure 4 shows that when the cutting temperature was stable, the temperature field distribution of the rake face of the five micro-textured tools was extracted by the post-processing of ABAQUS. The maximum temperature of the tool was concentrated in the local deformation area near the tool nose because this area was where plastic deformation and tool–chip friction were relatively concentrated. As the cutting temperature accumulates with the plastic deformation and friction of the workpiece, the temperature center shifts from the tool nose to the micro-texture. Through the comparative analysis, the micro-texture has a significant impact on the cutting temperature of the tool. Therefore, it could be seen that the maximum temperature of the non-textured tool is concentrated within 0.4 mm from the tool nose during the stable cutting; the maximum temperature reached 148 °C; the maximum cutting temperature of the micro-groove-parallel textured tool was 125.9 °C; and this temperature is the lowest among these cutting tools. Compared with the non-textured tool T0, the temperature of the tool T1 was reduced by 10.1%, while the temperatures of the tools T2, T3, T4, and T5 decreased by 12.2%, 14.9%, 6.8%, and 11.5%, respectively. Through the above analysis, it could be found that the reason for this may be that the micro-texture of the T3 tool is perpendicular to the direction of chip outflow, which reduces the length of tool–chip contact and friction and results in a decrease in cutting temperature.

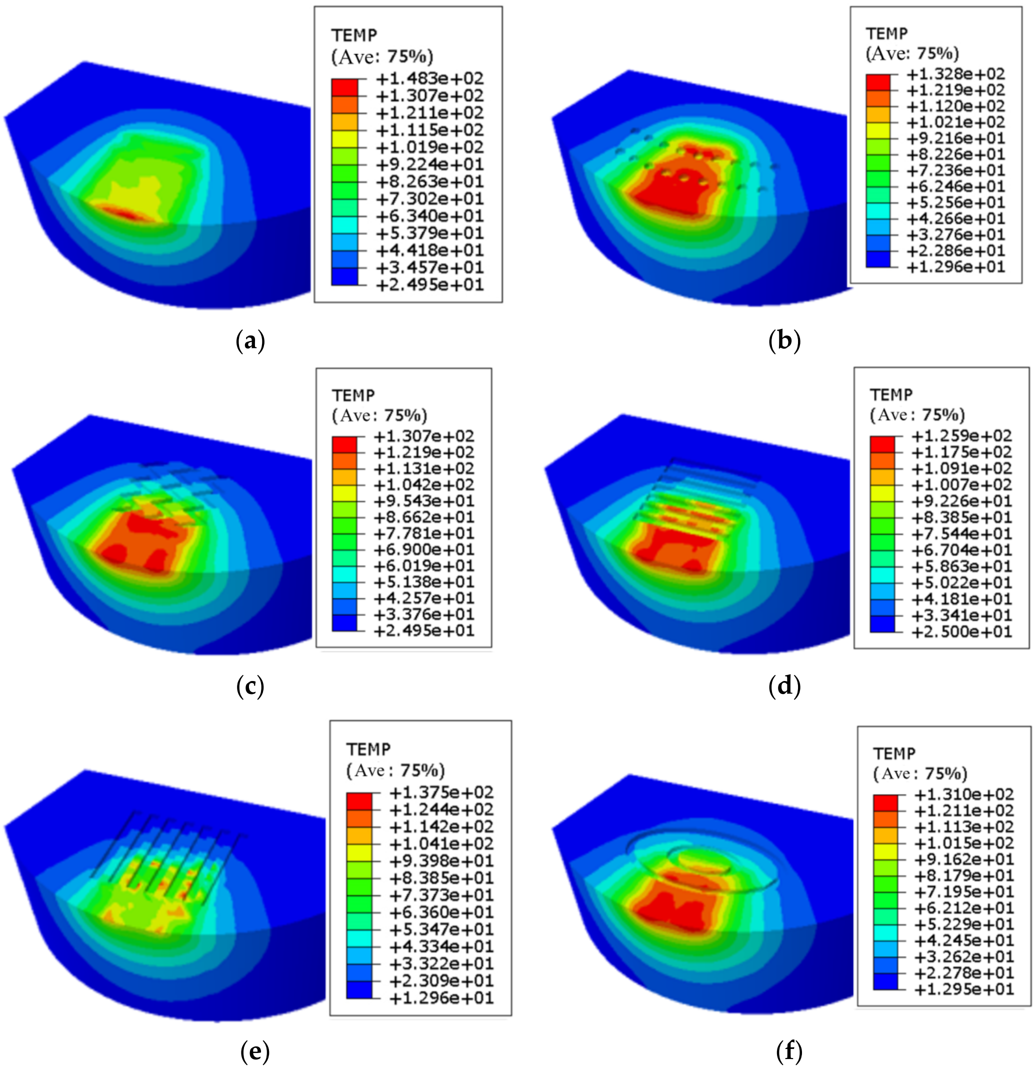

Figure 4. Distribution diagram of tool temperature field in the stable stage of the cutting temperature: (**a**) non-textured tool T0; (**b**) micro-pit texture tool T1; (**c**) micro-pyramids textured tool T2; (**d**) micro-groove-parallel textured tool T3; (**e**) micro-groove-vertical textured tool T4; and (**f**) micro-elliptical textured tool T5.

Figure 5 shows the changing curves of the temperatures of the tool nose when the analysis steps were 10, 20, 30, and 40 for the non-textured tool and the five micro-textured tools with different morphologies. In a complete analysis step of cutting, the cutting temperature of the tool nose tended to be stable after rising, and the temperature of the non-textured tool increased instantaneously after contacting the workpiece. With the increase in the analysis step, the curvature changed, and the rate slowed down between 25–40 steps; however, the heating speed was still faster than that of the micro-textured tool. The heating curves of the T1, T2, and T5 tools were roughly the same. Because of the small cutting parameters, the cutting area of the micro-texture placed on the rake face was roughly the same, the temperature change was not obvious, and the rising rate of the temperature was roughly distributed as T0 > T4 > T5 > T1 > T2 > T3. In step 40, it could be seen that the temperature did not increase or decrease linearly but oscillated around a stable value.

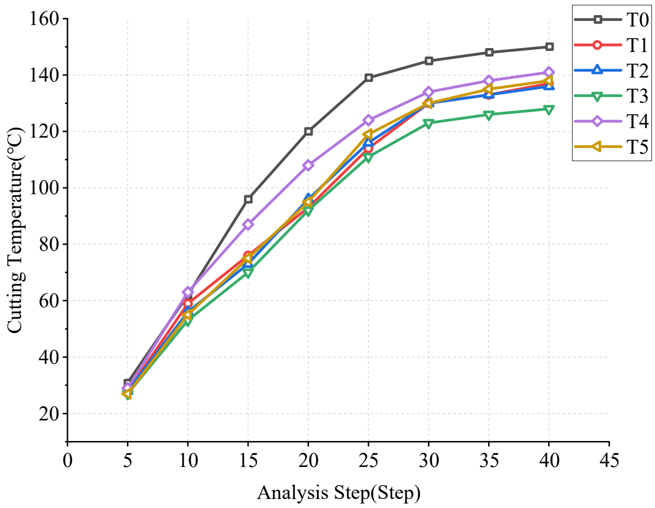

Figure 5. Temperature under different simulation analysis steps.

The overall local temperatures of the micro-textured tool were lower than those of the non-textured tool. The reason for the decrease in the temperature could be analyzed from the chip shape and the friction reduction mechanism of the micro-texture. On the one hand, the reduction in temperature was due to the increase in the unit chip curl rate, which was caused by the micro-textured tool. Compared with the non-textured tool, the chip was separated from the rake face of the tool earlier, which reduced the contact area of the friction pair. On the other hand, in the close contact area of the chips, the micro-texture made the chips form vacuum contact in their existing area, which was also an important factor in reducing the cutting temperature of the micro-textured tool. Being involved in the complexity of material failure and friction conditions in the actual cutting process, the simulation results were acceptable.

According to the cutting principle, the formation of the cutting heat was positively correlated with the contact length between the tool and chips, and the micro-grooves of tool T3 played two important roles in the formation of the chip. Firstly, continuous chips were divided into short segments, and the close contact only occurred at the peak of the micro-groove. Secondly, the micro-groove acted on the initial position of the chips flowing across the surface, making the micro-groove reduce the cutting heat caused by chip flow. Due to the small cutting parameters, the chips would immediately curl after flowing through the first deformation area of the micro-groove. When placed in parallel, the width of the micro-groove was small, and thus the contact area was smaller, which may be the reason why the micro-grooves parallel to the tool nose have better cooling performance.

4. Simulation Analysis of Cutting Temperature for Micro-Groove-Parallel Texture with Different Parameters

From the results of the simulation of different micro-texture morphologies above, the cooling effect of tool T3 was the most obvious. To further study the performance of tool T3 with different size parameters and select the micro-texture size parameters with the lowest cutting temperature, an orthogonal simulation scheme for the size parameters of tool T3 was designed and analyzed through simulation. The groove parameters of tool T3 were as follows: edge distance *A*, spacing *B*, width *C*1, and length *C*2 (meaning of parameters shown in Figure 1). During the simulation, the cutting parameters were set as follows: cutting speed v was 50 m/min, cutting depth a_p was 0.2 mm, and feed rate f was 0.2 mm/r. The simulation scheme of the relevant size parameters and tool nose temperature are shown in Table 5.

Table 5. Orthogonal simulation scheme of the tool T3.

Number	*A*/µm	*B*/µm	*C*1/µm	*C*2/µm	Cutting Temperature/°C
1	50	60	20	300	130
2	80	80	30	300	134
3	110	100	40	300	131
4	140	120	50	300	128
5	80	100	20	350	138
6	50	120	30	350	138
7	140	60	40	350	142
8	110	80	50	350	135
9	110	120	20	400	133
10	50	100	30	400	129
11	140	80	40	400	133
12	80	60	50	400	132
13	140	80	20	450	135
14	110	60	30	450	143
15	80	120	40	450	141
16	50	100	50	450	141

From Table 5, tool NO.4 has the lowest temperature and, therefore, the best cooling effect. Its size parameters are as follows: *A* is 140 µm, *B* is 120 µm, *C*1 is 50 µm, and *C*2 is 300 µm.

5. Turning Experiment

In this section, the micro-textured tools were used to cut GH4169 in spray cooling to verify the accuracy of the simulation of ABAQUS.

In the experiment, the CKA6140 machine tool was used for cutting, and the cutting material was a GH4169 bar with a size of Φ120 × 300 mm. The designed carbide micro-texture tools (micro-texture was processed on the rake face of inset CNMA120408-KR-3225 produced by Sandvik, coated with CVD TiCN+Al2O3+TiN) were used, the temperature-measuring equipment adopts artificial thermocouple method, standard thermocouple (WPNK-191) was used, and the cooling mode was spray cooling. The model of the composite spray cooling equipment is OoW129S. A specific cutting fluid was prepared for the experiment. The cutting fluid was added to the cutting fluid tank of OoW129S. The cutting fluid was vaporized under high pressure produced by an extra-linked air pump and sprayed into the cutting area, which cooled the cutting area. The nozzle flow rate of the spray device is 3.16 L/h, and the inlet pressure is 0.2 Mpa. In the experiment, the micro-textured tools listed in Table 2 were processed using a femtosecond laser, and the tool nose was partially enlarged, as shown in Figure 6.

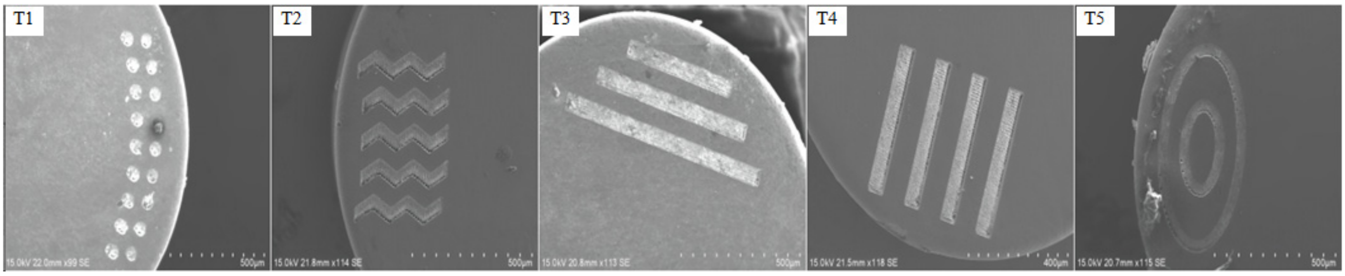

Figure 6. Enlarged views of micro-texture shapes of five tool noses.

5.1. Actual Temperature of the Cutting Area

5.1.1. Temperature Measuring Method and Processing Method

The measurement methods of temperature in the turning process are usually divided into contact and non-contact measurement methods. The specific measurement methods include the thermocouple method [27], infrared thermal imager method [28], radiation pyrometer method [29], and enhanced CCD method [30], in which thermocouple also includes artificial, semi-artificial, and natural thermocouple.

Since the cutting in this paper was carried out in spray cooling, and spray would cause the interference of the infrared ray and lead to inaccurate temperature measurement, the natural thermocouple method was used in this experiment to measure temperature.

Considering the influence of the strength of the micro-textured tool, the electric discharge machining [31] was used to drill the hole in the bottom side of the tool to measure the temperature near the rake face of the tool. As shown in Figure 7a, the distance between the thermocouple measuring area and the cutting area was 1 mm, and the diameter of the hole was 0.5 mm. Standard thermocouples were inserted into the hole and maintained the insulation between the thermocouples and the hole wall. In cutting, the thermocouples felt the temperature of the measuring point, and the potential value was measured by the instrument. Then, the temperature of the measuring point was obtained based on the thermocouple calibration curve. In the experiment, the sensing wire of the thermocouple can be directly inserted into the blind hole inside the tool and fixed by the resin coating. Figure 7b shows the drilling position of the micro-textured tool.

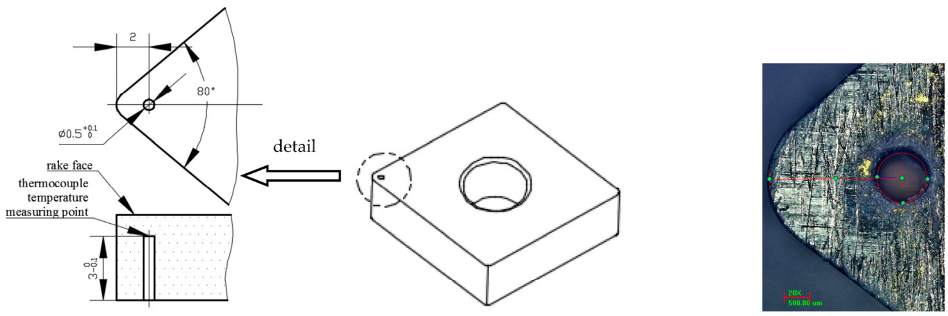

(**a**) (**b**)

Figure 7. Position of the temperature measurement point: (**a**) hole of the thermocouple; (**b**) the hole machined by EDM of the tool.

5.1.2. Derivation of Tool Nose Temperature

Because the thermocouple temperature measurement can only measure the temperature at a certain point the certain distance from the rake face, in order to eliminate this limitation of thermocouple temperature measurement, the inverse heat conduction method was used to find out the relationship between the temperature measured by the thermocouple and the actual temperature of the tool nose. The specific flow chart of the inverse heat conduction method is shown in Figure 8.

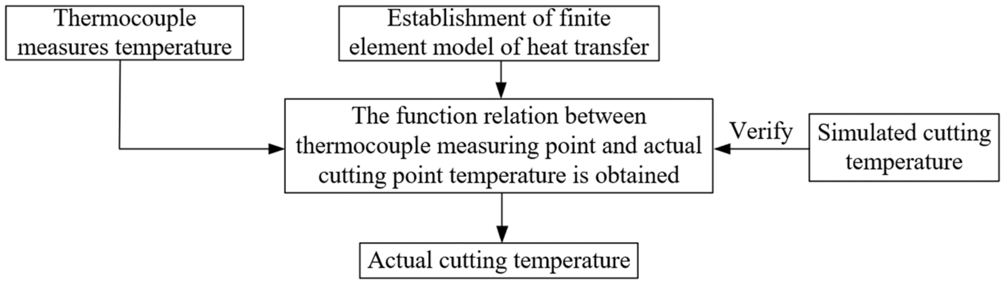

Figure 8. Flow chart of heat conduction inverse method.

The heat transfer model was established in ANSYS. As shown in Figure 9, only the tool nose and its adjacent area participated in the whole cutting process, and the cube of 0.7 mm × 0.7 mm × 1 mm was divided at the tool nose. The upper surface of the cube was used as the cutting area, the lower surface was used as the measurement area of the thermocouple, and the temperature obtained in the cutting area was the cutting temperature.

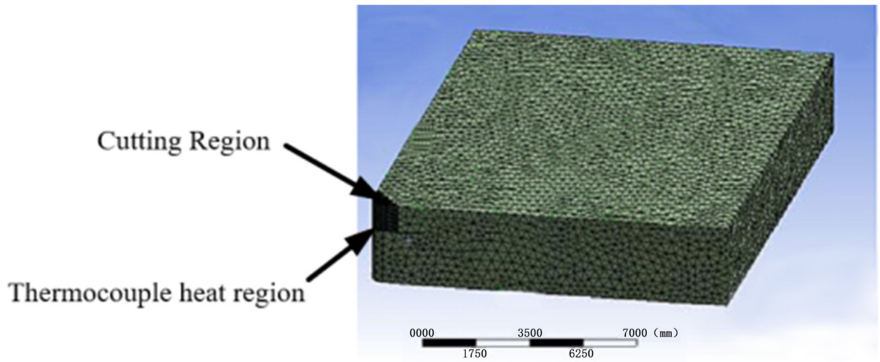

Figure 9. Heat-transfer model.

In the analysis of the heat-transfer process, the main step was the temperature transfer of the small cube cut from the tool nose. Then, the meshes of the small cube part were refined to improve the accuracy of the calculation. The properties of the carbide material are shown in Table 6. After applying the cutting temperatures of 200 °C, 250 °C, 300 °C, and 350 °C in the cutting area, the temperatures in the thermocouple measurement area can be obtained, respectively. Table 7 shows the comparison between the measured temperatures of the thermocouple and the actual cutting temperatures.

Table 6. Properties of cemented carbide.

Materials	Carbide
Thermal Conductivity (W/M·°C)	71
Density (Kg/m^3)	15,600
Specific Heat(J/Kg·°C)	452

Table 7. Heat transfer results.

Number	Tool Nose Temperature *Y*	Measuring Temperature *X*
1	200	123.98
2	250	167.47
3	300	214.97
4	350	256.90

The data in Table 7 were fitted by MATLAB, and the final equation of the relationship between the actual temperature of the tool nose and the measured temperature is as follows:

$$Y = 0.00021873X^2 + 1.0366X + 68.6841 \quad (2)$$

where X was the temperature of the measurement area of the thermocouple, and Y was the temperature of the tool nose in the cutting area. Experiments showed that the temperature measured by the thermocouple in dry cutting was 136 °C; substituting this into the above formula, X obtained that Y was equal to 213.71 °C, which was the temperature of the tool nose. Under the same cutting parameters, the cutting temperature of the simulation was 197 °C by using DEFORM. Compared with the results of DEFORM, the results obtained by substituting the temperature measured by the thermocouple into the formula and the error of the simulation results relative to the experimental results is 7.51%, which was within the acceptable range. In conclusion, the fitted quadratic function is more accurate.

5.2. Cutting Experiments with Different Micro-Texture Shapes

Figure 10 shows the machining site of the micro-textured tools when cutting GH4169 in spray cooling. The morphologies and size parameters of the micro-textured tools used in the experiments were consistent with those in the simulation.

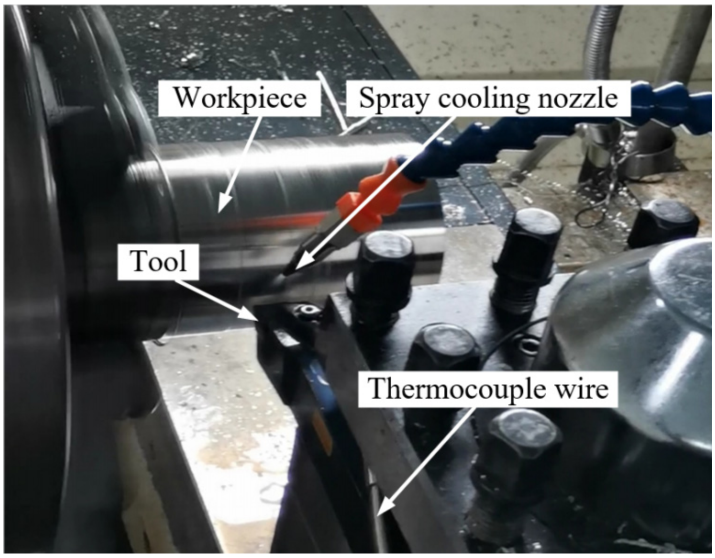

Figure 10. Experimental setup of cutting GH4169 in spray cooling.

As shown in Figure 11, the actual temperature curves of the tool noses were obtained when cutting GH4169 under the conditions of cutting parameters that v was 50 m/min, f was 0.2 mm/r, and a_p was 0.2 mm. It can be seen from the curves that the cutting temperatures of the five micro-textured tools were lower than that of the non-textured tool, and the cooling effects of different micro-textured tools were different for the five micro-textured tools. At the beginning of the cutting, the temperature rose rapidly, and the temperature curves in the later period showed a trend of smooth rising. Among them, the highest cutting temperatures of T0, T1, T2, T3, T4, and T5 were 82 °C, 68 °C, 75 °C, 63 °C, 65 °C, and 69 °C, respectively. Compared with the non-textured tool, the cooling rates of the micro-textured tools were 17%, 9%, 23%, 21%, and 15%, respectively. The micro-textured tool T3 had the best cooling effect.

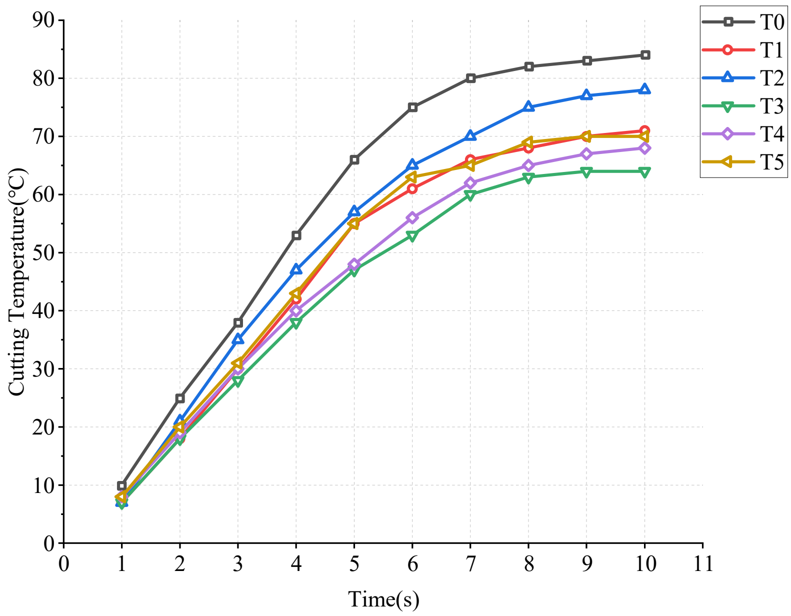

Figure 11. Temperature of tool noses with different shapes at different time points.

5.3. Cutting Experiment of Micro-Groove-Parallel Texture Tools with Different Size Parameters

In order to verify the accuracy of the simulation model of cutting GH4169 with the micro-textured tools designed in Table 5 and to explore the influence of the parameters A, B, $C1$, and $C2$ of the micro-texture of tool T3 on the cutting temperature, the tools designed in Table 5 were processed, and several tool noses were locally enlarged, as shown in Figure 12. The cutting experiments on GH4169 were carried out using these tools, with the same cutting parameters as the simulation; that is, v was 50 m/min, f was 0.2 mm/r, and a_p was 0.2 mm.

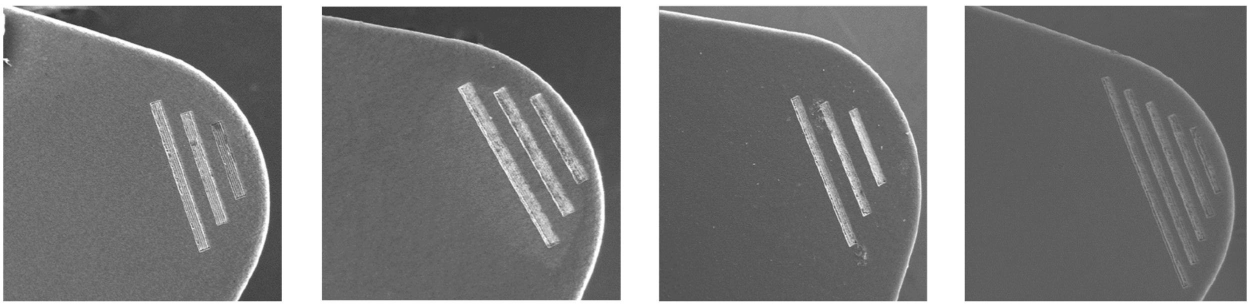

Figure 12. Micro-groove-parallel textured tools with different size parameters.

Figure 13 shows the tool nose temperature measurement of the T3 tool under the different micro-texture size parameters. From Figure 13, it can be seen that under the condition of spray cooling, the cutting temperature of tool No. 4 is the lowest, with a value of 56 °C. The size parameter A of tool No. 4 is 140 µm, and B is 120 µm. $C1$ is 50 µm, and $C2$ is 300 µm. The results are consistent with the optimization of simulation data, proving the accuracy of the simulation model. It was also proven that the optimal size parameter combination of the groove which parallels the tool nose of the micro-textured tools is as follows: the distance from the groove to the tool nose is 140 µm, the space between grooves is 120 µm, the width of the groove is 50 µm, and the length of the groove is 300 µm.

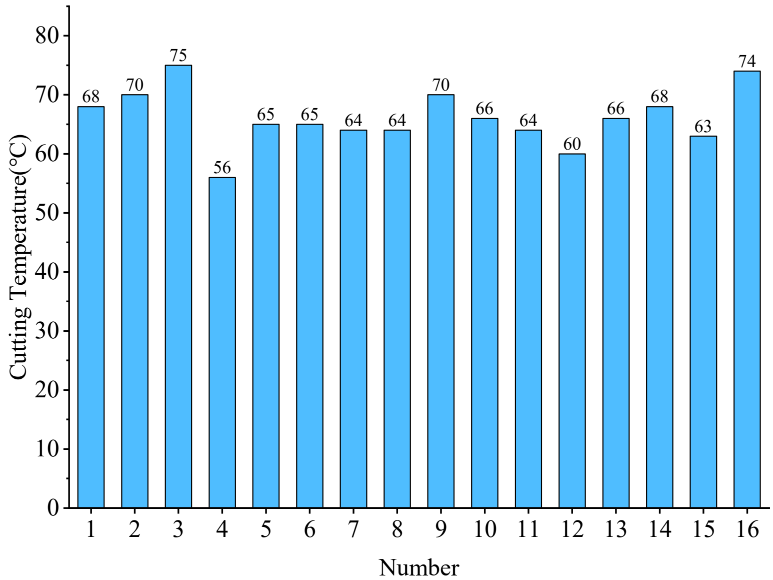

Figure 13. Temperature of tool nose with different size parameters of micro-groove-parallel textured tools.

In cutting GH4169, micro-textured tools can reduce cutting temperature. The best cooling morphology is T3. Firstly, in reference [16], when cutting AISI 1045, compared with the non-textured tools, the cutting temperature of the micro-textured tools was reduced by 21.7%, while the cutting temperature of tool T3 (linear groove parallel to the tool nose) in cutting GH4169 was reduced by 23% in this paper. Secondly, in reference [20], when cutting Al7076-T6, the parameters of micro-grooves are 80 μm, 110 μm, and 10 μm, while the optimal parameters *A*, *B*, and *C*1, in this paper for T3 cutting GHH4169, are 140 μm, 120 μm, and 50 μm, respectively. Finally, the same cutting parameters were adopted in both the simulation and experiment of this paper, and further research can be conducted on the optimal match between micro-textures and cutting parameters.

6. Conclusions

This paper studied the cutting temperature of micro-textured tools when cutting GH4169 in spray cooling. The research was conducted in finite element simulations and experiments. The influence of micro-textures with different morphologies and size parameters on the cutting temperature was revealed. The optimized morphology and size parameters of micro-textures were obtained. The following conclusions were drawn:

(1) Compared with non-textured tools, the use of micro-textured tools in cutting reduced both the average cutting temperature and the temperature at the tool nose. This results from two factors. On the one hand, the micro-textured tools increase the curl rate of the unit chip, which leads to an earlier separation of the chip from the rake face of the tool, thus reducing the contact area of the friction pair and lowering the cutting temperature. On the other hand, in the area where the chips are in close contact with the rake face, the micro-texture forms a vacuum contact, and it also means the existence of the vacuum contact becomes an important factor in cutting temperature reduction;

(2) Furthermore, the morphology of micro-textures has an effect on temperature reduction. Among the five designed morphologies, the comprehensive cooling performance of T3 (linear groove parallel to the tool nose) is significantly superior to the other morphologies. Compared with the non-textured tools, the temperature reduction in T3 is 23%, and those of T1, T2, T4, and T5 are 17%, 9%, 21%, and 15%, respectively;

(3) In addition, the size parameters of micro-textures have an effect on temperature reduction as well. Among the 14 combinations of dimensional parameters designed

for T3, the best combination with the lowest cutting temperature is as follows: *A* is 140 μm, *B* is 120 μm, *C*1 is 50 μm, and *C*2 is 300 μm;

(4) Experiments were conducted in the same working conditions as the simulation. Since the experimental results conformed to those of the simulation analysis, it can verify the accuracy and reliability of the simulation model.

Author Contributions: Methodology, X.F. (Xinmin Feng); software, X.F. (Xiwen Fan); validation, J.H.; writing—original draft preparation, X.F. (Xinmin Feng); writing—review and editing, J.W. All authors have read and agreed to the published version of the manuscript.

Funding: This research was financially supported by the National Science Foundation of China (Grant No. 51675144).

Data Availability Statement: Not applicable.

Conflicts of Interest: The authors declare no conflict of interest.

References

1. Hao, Z.; Yang, S.; Fan, Y.; Lu, M. Machining characteristics of cutting Inconel 718 with carbide tool. *Int. J. Mater. Prod. Technol.* **2019**, *58*, 275–287. [CrossRef]
2. Shi, L.; Zhang, C. Experimental research on turning of superalloy GH4169 under high pressure cooling condition. *Integr. Ferroelectr.* **2020**, *207*, 75–85. [CrossRef]
3. Pan, L.; Wu, Z.R.; Fang, L.; Song, Y.D. Investigation of surface damage and roughness for nickel-based superalloy GH4169 under hard turning processing. *Proc. Inst. Mech. Eng. Part B J. Eng. Manuf.* **2020**, *234*, 679–691. [CrossRef]
4. Li, J.; Wang, X.; Qiao, Y.; Fu, X.; Guo, P. Experimental and simulation of low-temperature cutting of nickel based alloy Inconel 718 using liquid nitrogen cooling. *J. Mech. Eng.* **2020**, *56*, 61–72.
5. Li, L.; Wu, M.; Liu, X.; Cheng, Y.; Yu, Y. Experimental study of the wear behavior of PCBN Inserts during cutting of GH4169 superalloys under high-pressure cooling. *Int. J. Adv. Manuf. Technol.* **2018**, *95*, 1941–1951. [CrossRef]
6. Zhang, Y.; Wu, M.; Liu, K. Optimization research of machining parameters for cutting GH4169 based on tool vibration and surface roughness under high-pressure cooling. *Materials* **2021**, *14*, 7861. [CrossRef]
7. Shu, S.; Zhang, Y.; He, Y.; Zhang, H. Design of a novel turning tool cooled by combining circulating internal cooling with spray cooling for green cutting. *J. Adv. Mech. Des. Syst. Manuf.* **2021**, *15*, 1–11. [CrossRef]
8. Xie, F.; Lei, X. The influence of bionic micro-texture's surface on tool's cutting performance. In *Key Engineering Materials*; Trans Tech Publications Ltd.: Wollerau, Switzerland, 2016; pp. 1155–1162.
9. Ozturk, E. FEM and statistical-based assessment of AISI-4140 dry hard turning using micro-textured insert. *J. Manuf. Process.* **2022**, *81*, 290–300. [CrossRef]
10. Yu, X.; Wang, Y.; Lv, D. Study on machining characteristics with variable distribution density micro-texture tools in turning superalloy GH4202. *Int. J. Adv. Manuf. Technol.* **2022**, *123*, 187–197. [CrossRef]
11. Zhang, K.; Li, Z.; Wang, S.; Wang, P.; Zhang, Y.; Guo, X. Study on the cooling and lubrication mechanism of magnetic field-assisted Fe_3O_4@CNTs nanofluid in micro-textured tool cutting. *J. Manuf. Process.* **2023**, *85*, 556–568. [CrossRef]
12. Rao, C.M.; Rao, S.S.; Herbert, M.A. Development of novel cutting tool with a micro-hole pattern on PCD insert in machining of titanium alloy. *J. Manuf. Process.* **2018**, *36*, 93–103. [CrossRef]
13. Zhang, J.; Yang, H.; Chen, S.; Tang, H. Study on the influence of micro-textures on wear mechanism of cemented carbide tools. *Int. J. Adv. Manuf. Technol.* **2020**, *108*, 1701–1712. [CrossRef]
14. Liu, X.; Liu, Y.; Li, L.; Tian, Y. Performances of micro-textured WC-10Ni (3) Al cemented carbides cutting tool in turning of Ti6Al4V. *Int. J. Refract. Met. Hard Mater.* **2019**, *84*, 104987. [CrossRef]
15. Wu, Z.; Bao, H.; Liu, L.; Xing, Y.; Huang, P.; Zhao, G. Numerical investigation of the performance of micro-textured cutting tools in cutting of Ti-6Al-4V alloys. *Int. J. Adv. Manuf. Technol.* **2020**, *108*, 463–474. [CrossRef]
16. Sun, J.; Zhou, Y.; Deng, J.; Zhao, J. Effect of hybrid texture combining micro-pits and micro-grooves on cutting performance of WC/Co-based tools. *Int. J. Adv. Manuf. Technol.* **2016**, *86*, 3383–3394. [CrossRef]
17. Feng, Y.; Zhang, J.; Wang, L.; Zhang, W.; Tian, Y.; Kong, X. Fabrication techniques and cutting performance of micro-textured self-lubricating ceramic cutting tools by in-situ forming of Al_2O_3-TiC. *Int. J. Refract. Met. Hard Mater.* **2017**, *68*, 121–129. [CrossRef]
18. Olleak, A.; Özel, T. 3D Finite element modeling based investigations of micro-textured tool designs in machining titanium alloy Ti-6Al-4V. *Proced. Manuf.* **2017**, *10*, 536–545. [CrossRef]
19. Yang, S.; Su, S.; Liu, X.; Han, P. Study on milling temperature of titanium alloy with micro-textured ball end milling cutter under radius of blunt edge. *Appl. Sci.* **2020**, *10*, 587. [CrossRef]
20. Li, K.; Du, J.; Liu, L.; Shen, F.; Ma, L.; Pang, M. Effect of texture parameters on main cutting Force and temperature of cutting tools. *Tool Eng.* **2019**, *53*, 42–46.
21. Arulkirubakaran, D.; Senthilkumar, V.; Kumawat, V. Effect of micro-textured tools on machining of Ti-6Al-4V alloy: An experimental and numerical approach. *Int. J. Refract. Met. Hard Mater.* **2016**, *54*, 165–177. [CrossRef]

22. Wang, B.; Zhang, J.Y.; Wu, C.L.; Deng, W.J. A numeric investigation of rectangular groove cutting with different lateral micro textured tools. In *Key Engineering Materials*; Trans Tech Publications Ltd.: Wollerau, Switzerland, 2016; Volume 693, pp. 697–703.
23. Moakhar, S.; Hentati, H.; Barkallah, M.; Louati, J.; Haddar, M. Parametric study of aluminum bar shearing using Johnson-Cook material modeling. *Proc. Inst. Mech. Eng. Part B J. Eng. Manuf.* **2021**, *235*, 1399–1411. [CrossRef]
24. Wang, Z.; Lv, Y. Simulation Study on cutting force of high temperature alloy GH4169 based on ABAQUS. *Light Ind. Mach.* **2019**, *37*, 42–45.
25. İynen, O.; Ekşi, A.K.; Akyıldız, H.K.; Özdemir, M. Real 3D turning simulation of materials with cylindrical shapes using ABAQUS/Explicit. *J. Braz. Soc. Mech. Sci. Eng.* **2021**, *43*, 374. [CrossRef]
26. Feng, X.; Dong, Q.; Hu, J. Simulation and experiment analysis of the cutting force of high-speed turning GH4169 with spray cooling. *J. Mach. Des.* **2021**, *38*, 74–79.
27. Zhou, M.; Kulenovic, R.; Laurien, E.; Kammerer, M.C.; Schuler, X. Thermocouple measurements to investigate the thermal fatigue of a cyclic thermal mixing process near a dissimilar weld seam. *Nucl. Eng. Des.* **2017**, *320*, 77–87. [CrossRef]
28. Qi, Z.; Guohe, L.; Yong, S.; Fei, S. Experimental study on emissivity setting before precise temperature measurement of SiCp/Al cutting by infrared thermal imager. *Infrared Laser Eng.* **2022**, *51*, 179–188.
29. De Lucas, J.; Segovia, J.J. Measurement and Analysis of the Temperature Gradient of Blackbody Cavities, for Use in Radiation Thermometry. *Int. J. Thermophys.* **2018**, *39*, 57. [CrossRef]
30. Luo, T.; Zhang, Q. Application of CCD non-contact detection technology in industrial production. *New Technol. New Prod. China* **2021**, 69–71. [CrossRef]
31. Rex, N.A.; Vijayan, K. Machining of microholes in Ti-6Al-4V by hybrid electro-discharge machining process. *J. Braz. Soc. Mech. Sci. Eng.* **2022**, *44*, 129. [CrossRef]